Available online at www.sciencedirect.com

ScienceDirect

Procedia Engineering 116 (2015) 623 – 630

Procedia Engineering

www.elsevier.com/locate/procedia

8th International Conference on Asian and Pacific Coast (APAC 2015)

CFD Simulations to Determine Wave Forces on a Row of Cylinders

Arun Kamath[a,*], Hans Bihs[a], Mayilvahanan Alagan Chella[a], Øivind A. Arntsen[a]

[a]*Department of Civil and Transport Engineering, Norwegian University of Science and Technology, Trondheim 7491, Norway*

Abstract

The open source Computational Fluid Dynamics (CFD) model REEF3D is used to simulate interaction of low steepness linear waves and high steepness 5*th*-order Stokes waves with a single cylinder and linear arrays of two, three, four and five large cylinders. The wave forces on any cylinder in the array is seen to generally increase with the inclusion of additional downstream cylinders in both cases. The wave forces on the downstream cylinders also reduce along the length of the array and the most downstream cylinder experiences the least forces in the array. The formation of standing waves in between the cylinders is observed in the case of low steepness incident waves. The wave forces on the most downstream cylinder in the array is almost equal to the force on a single cylinder in the case of low steepness incident waves and less than the force on a single cylinder in the case of high steepness incident waves.

Peer- Review under responsibility of organizing committee , IIT Madras , and International Steering Committee of APAC 2015

Keywords: cylinder array, wave forces, wave diffraction, CFD, REEF3D

1. Introduction

The interaction of waves with large bodies results in significant modification of the wave field and wave induced processes such as wave radiation and wave diffraction occur. The evaluation of wave diffraction effects due to a large object and its influence on the free surface around it and wave forces on other objects in the neighborhood involves accounting for multiple wave reflection and diffraction processes. These processes can lead to wave near-trapping, which is a resonance-type phenomenon where large forces are experienced by cylinders placed in proximity for certain incident wavelengths [1]. Many researchers have dealt with the problem of wave diffraction around multiple large cylinders arranged in a closely spaced group [2] [3] [4] [5] and for the case of linear arrays of cylinders [6] under the assumption of linear water waves using potential theory. These studies have provided a large amount of information on wave forces on cylinders in groups for different incident wave conditions, however they are limited by the assumptions of small amplitude waves, inviscid fluid and irrotational flow in potential theory. It has also been reported that the large wave forces on the cylinders as predicted by the analytical formulae could not be observed in experiments [7] [8]. According to [7] and [8], the resonance effect is very sensitive to deviations from the ideal wave field assumed in theory and is difficult to replicate these in experiments. Also a small level of disorder in the arrangement of the cylinders, of the order of 0.5% of the cylinder spacing, disrupt the wave near-trapping phenomenon [9]. Thus, there

* Corresponding author. Tel.: +47-735-94640 ; fax: +47-735-97021.
E-mail address: arun.kamath@ntnu.no

Peer- Review under responsibility of organizing committee , IIT Madras , and International Steering Committee of APAC 2015
doi:10.1016/j.proeng.2015.08.334

still exists a gap in the knowledge regarding wave interaction with groups of large cylinders. In addition, there is little literature dealing with the variation of the free surface in the vicinity of the cylinders and the effect of high steepness incident waves.

Computational Fluid Dynamics (CFD) modeling solves the fluid flow problem using the Navier-Stokes equations, where the hydrodynamics can be calculated in detail with few assumptions, providing results with good representation of the flow physics. In current literature, many researchers have employed CFD modeling to study wave propagation and hydrodynamics in the context of ocean and coastal engineering [10] [11] [12] [13] [14]. The physical processes and the free surface features in the vicinity of the objects can be studied in detail using CFD simulations, including interaction of high steepness waves, non-linear wave-body and wave-wave interactions.

This paper presents the wave interaction with multiple cylinders arranged in a linear array for both low and high steepness waves using the open source CFD model REEF3D [13]. The wave interaction with a single cylinder is first carried out for both low and high incident waves and then the interaction with two, three, four and five cylinders placed in a tandem is studied. The wave forces on each of the cylinders in the different cases is studied along with the free surface in the vicinity of the cylinders. The effect of multiple neighboring cylinders and the incident wave steepness is discussed.

2. Numerical Model

The CFD model REEF3D solves the incompressible Reynolds Averaged Navier-Stokes (RANS) equations together with the continuity equation to solve the fluid flow problem:

$$\frac{\partial u_i}{\partial x_i} = 0 \tag{1}$$

$$\frac{\partial u_i}{\partial t} + u_j \frac{\partial u_i}{\partial x_j} = -\frac{1}{\rho}\frac{\partial p}{\partial x_i} + \frac{\partial}{\partial x_j}\left[(\nu + \nu_t)\left(\frac{\partial u_i}{\partial x_j} + \frac{\partial u_j}{\partial x_i}\right)\right] + g_i \tag{2}$$

where u is the velocity, ρ is the density of the fluid, p is the pressure, ν is the kinematic viscosity, ν_t is the eddy viscosity and g the acceleration due to gravity.

The pressure is treated with the projection method [15] and the resulting Poisson pressure equation is solved by a preconditioned BiCGStab [16] iterative solver. The two equation $k-\omega$ model [17] is used for turbulence modeling. The unphysical overproduction of turbulence in a numerical wave tank due to the high strain nature of wave propagation is avoided using eddy viscosity limiters as shown by [18]. The large difference in the density of water and air at the interface in a two-phase model leads to overproduction of turbulence at the interface. Turbulence damping at the interface is carried out using the procedure by [19] at the interface using the Dirac delta function.

The level set method [20] is used to obtain a sharp interface between water and air. The level set function is reinitialized after every time step using the partial differential equation-based procedure by [21] to maintain the signed distance property of the level set function after convection. The convective terms of the RANS equation are discretized using the finite difference conservative fifth-order WENO scheme [22]. The level set function ϕ, turbulent kinetic energy k and the specific turbulent dissipation rate ω are discretized using the Hamilton-Jacobi formulation of the WENO scheme [23]. The WENO scheme is numerically stable, a minimum third-order accurate even in the presence of large gradients and preserves the extrema in the solution. Time advancement is carried out using a fractional step scheme [24]. The numerical stability of the simulation is ensured while maintaining an optimal time step satisfying the CFL criterion using an adaptive time stepping approach.

A Cartesian grid is used for spatial discretization in the numerical model, providing for straightforward implementation of higher order discretization schemes. The numerical grid is staggered with the pressure at the cell center and the velocities at the cell faces resulting in a tight coupling of the pressure and velocity. The local directional ghost cell immersed boundary method [25] extended to three dimensions is employed to handle irregular boundaries. REEF3D is fully parallelized using the domain decomposition strategy and MPI (Message Passing Interface).

The numerical wave tank in REEF3D uses the relaxation method with relaxation functions presented by [11] to generate and absorb waves. The relaxation function is used to moderate the computational values of velocity and free surface with the analytical values prescribed by the wave theory to smoothly generate waves in the wave generation

zone. The waves propagate in the working zone of the tank and are absorbed at the numerical beach at the other end of the tank, where the computational values are smoothly reduced to zero to remove the wave energy from the numerical wave tank with out reflections back into the working zone. the relaxation function at the generation zone also absorbs the reflected waves from the working zone propagating towards the generation zone and prevents them from affecting the generated waves. Further details regarding the numerical model are presented in [13] and[26].

3. Results and Discussion

The numerical wave tank is validated for wave generation and propagation for waves of high and low steepnesses [13] [26] [14] and for the computation of wave forces [27]. The following sections present the results for wave forces evaluated for a single cylinder and linear arrays of two, three, four and five cylinders of diameter $D = 0.5$ m in a water depth $d = 0.5$ with incident waves of wavelength $L = 2.0$ m for heights $H = 0.006$ m (linear wave theory) and $H = 0.15$ m (5*th*-order Stokes wave theory). The numerical wave tank is 15-20 m long, 5 m wide and 1 m high, with a grid size $dx = 0.025$ m resulting in 4.78-6.33 million grid cells. The cylinders are placed at a constant center-to-center distance of 0.8 m from each other in the linear array to study the wave interaction with closely spaced cylinders, where the spacing between the cylinders is less than half of the incident wavelength.

3.1. Interaction of low steepness incident waves with an array of cylinders

At first, linear waves of height $H = 0.006$ m and wavelength $L = 2.0$ m with a wave steepness of $H/L = 0.003$ are incident on a single cylinder in the numerical wave tank. The computed forces (F_0) on the cylinder are compared with predictions from MacCamy-Fuchs theory (F_t) and a good agreement is seen in Fig. (1a). The numerically obtained wave force $F_0 = 9.26$ N is used to scale the wave forces on the cylinders in the other configurations simulated in this section. Further, simulations are carried out with two, three, four and five cylinders placed in tandem. The computed wave forces on each of the cylinders in all the cases are presented in Fig. (1b).

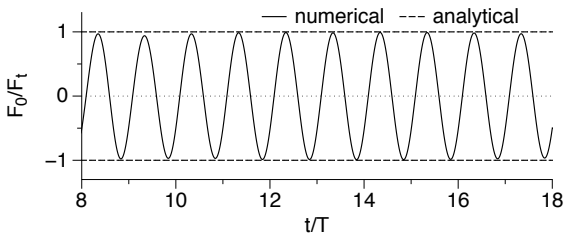

(a) Comparison of numerical and theoretical wave forces on a single cylinder

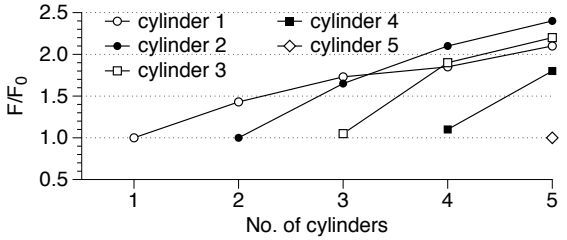

(b) Variation of wave forces on the different cylinders

Fig. 1: Wave forces on a single cylinder and in arrays of 1 − 5 cylinders for low steepness waves with $H = 0.006$ m and $L = 2.0$ m

The wave forces on the first cylinder in the array increases from $1.43F_0$ to $2.1F_0$ as the number of cylinders in the array is increased from two to five, though the rate of increase is reduced on the addition of the fourth cylinder. Cylinder 2 experiences the same force as that on a single cylinder in the absence of any downstream cylinders but experiences higher forces as the number of downstream cylinders is increased, with a wave force of $2.4F_0$ when placed in a five cylinder array. The wave force on cylinder 3 is $1.05F_0$ in the absence of downstream cylinders and increases to $1.9F_0$ and $2.2F_0$ in the presence of one and two additional cylinders downstream. A wave force of $1.1F_0$ is computed for cylinder 4 in the absence of downstream cylinders and an increased force of $1.8F_0$ is obtained when the fifth cylinder is added to the array. In the case of the fifth cylinder, the wave force acting on it is the same as that on a single cylinder, F_0.

Thus, the wave force on a cylinder is seen to increase with the addition of downstream cylinders for all the cases simulated. In each of the cases, the most downstream cylinder experiences almost the same wave force as that on a single cylinder. In order to obtain a better understanding of the wave diffraction process in these cases, the free surface

elevations around the cylinders during the incidence of a wave crest on the first cylinder is presented in Fig. (2). Due to diffraction of the incident waves by the cylinders, the wave field is redistributed in such a way that the largest change in free surface occurs around cylinders 2 and 3 in the presence of downstream cylinders. In the case of cylinder 2, Figs. (2b), (2c) and (2d) show the formation of simultaneously occurring, deep troughs and crests in front and behind the cylinder. This points towards large changes in pressure around cylinder 2 when placed in a three, four and five cylinder array resulting in the highest wave forces in the array acting on cylinder 2 for the final two cases. In the absence of an additional downstream cylinder, the diffraction effects on a cylinder are reduced and the change in pressure around the most downstream cylinder is lower, resulting in forces similar to that on a single cylinder. This is supported by the lower changes in the free surface elevation contours seen in Fig. (2) around the most downstream cylinder. The effect of diffraction leading to the bending of the incident wavefront and the propagation of the arched waves is seen also seen in the figures and this effect is stronger with a higher number of cylinders in the array.

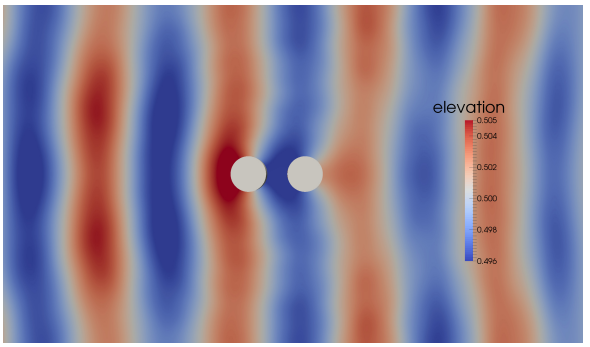

(a) two tandem cylinders

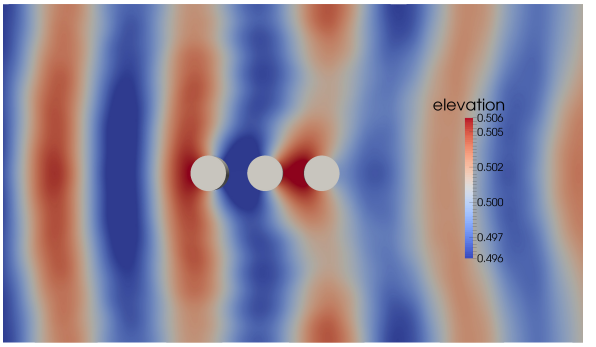

(b) three tandem cylinders

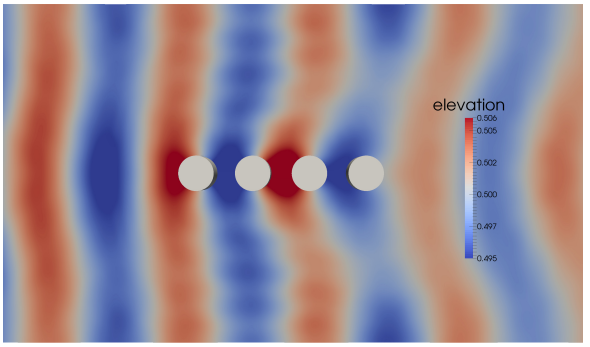

(c) four tandem cylinders

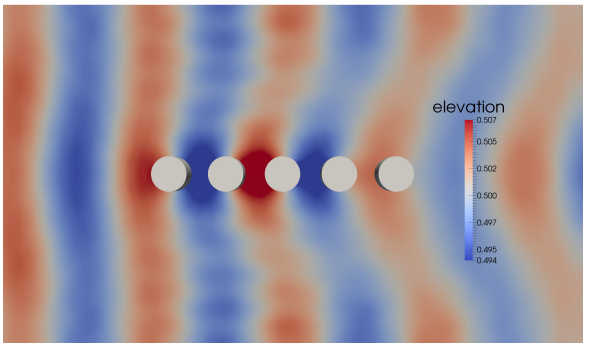

(d) five tandem cylinders

Fig. 2: Free surface elevations in the vicinity of the cylinders in different arrangements for low steepness incident waves ($H/L = 0.003$) with $H = 0.006$ m and $L = 2.0$ m at $t/T = 20$

3.2. Interaction of high steepness incident waves with an array of cylinders

Fifth-order Stokes waves of height $H = 0.15$ m and wavelength $L = 2.0$ m with wave steepness $H/L = 0.075$ are generated in the numerical wave tank and the computed wave force on a single cylinder is presented in Fig. (3a). The computed force on a single cylinder $F_0 = 150.0$ N is used to scale the wave forces computed for the different linear arrays of cylinders. The wave forces computed for each cylinder in the different linear arrays is presented in Fig. (3b).

The wave force on the first cylinder in the array increases with increase in the number of downstream cylinders, but the rate of increase is reduced with every additional downstream cylinder. The computed wave force on cylinder 1 is $1.25F_0$ with one downstream cylinder and increases to $1.53F_0$ with four downstream cylinders. In the case of

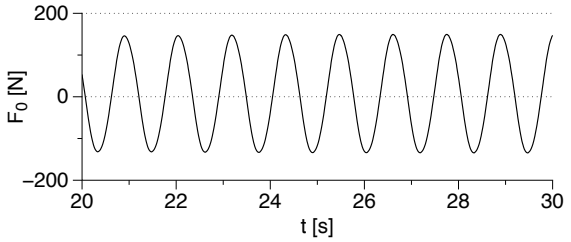

(a) Numerically computed wave forces on a single cylinder

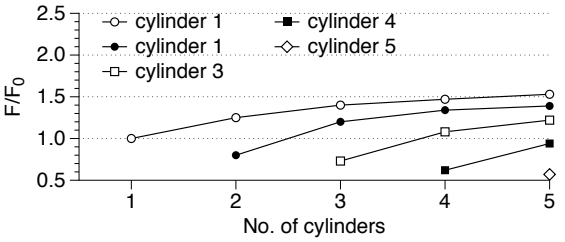

(b) Variation of wave forces on the different cylinders

Fig. 3: Wave forces on a single cylinder and in arrays of $1-5$ cylinders for high steepness waves with $H = 0.15$ m and $L = 2.0$ m

cylinder 2, the wave forces increases from $0.80F_0$ without any downstream cylinders to $1.40F_0$ with three downstream cylinders. The rate of increase of wave forces follows a similar pattern as that for cylinder 1 but with lower values for wave forces. Similarly, cylinder 3 and cylinder 4 experience wave forces of $0.73F_0$ and $0.62F_0$ respectively without any downstream cylinders. The wave forces on cylinders 3 and 4 increase to $1.22F_0$ and $0.94F_0$ respectively when they are placed in a five cylinder linear array. The computed wave force on cylinder 5 is $0.57F_0$ and it experiences the least force in the cylinder array.

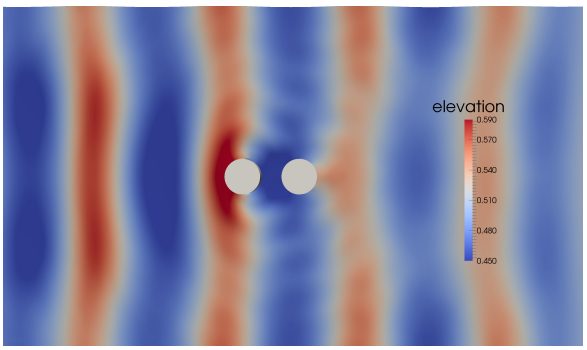

(a) two tandem cylinders

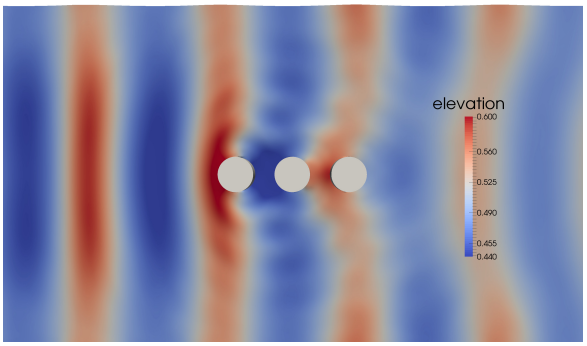

(b) three tandem cylinders

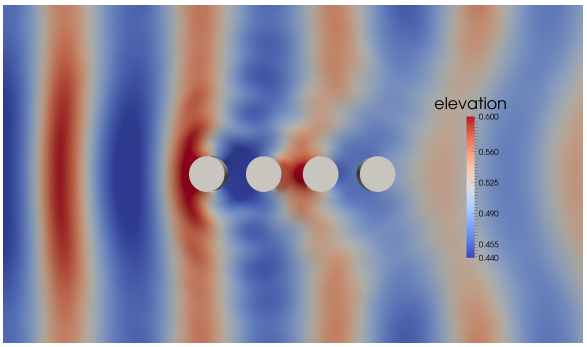

(c) four tandem cylinders

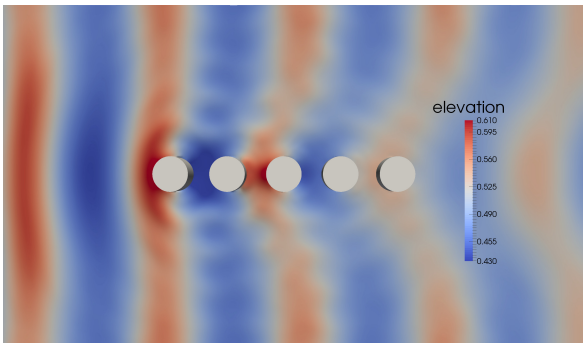

(d) five tandem cylinders

Fig. 4: Free surface elevations in the vicinity of the cylinders in different arrangements for high steepness incident waves ($H/L = 0.075$) with $H = 0.075$ m and $L = 2.0$ m at $t/T = 20$

In the case of high steepness incident waves, the wave forces on the cylinders are seen to increase on increasing the number of downstream cylinders, but the increase in the wave force is reduced significantly when additional cylinders

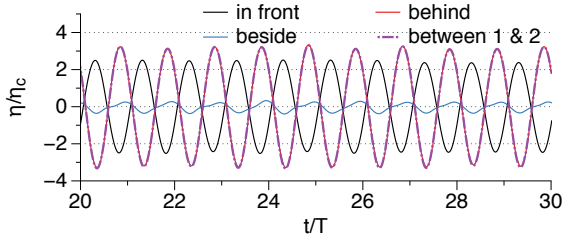

(a) cylinder 1, $H/L = 0.003$

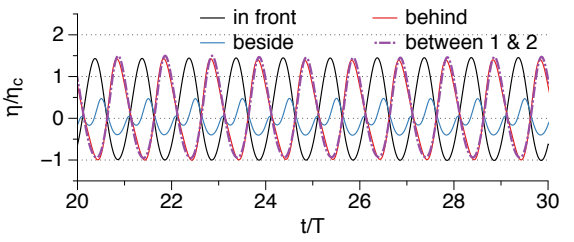

(b) cylinder 1, $H/L = 0.075$

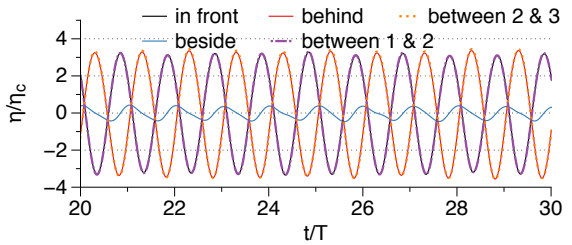

(c) cylinder 2, $H/L = 0.003$

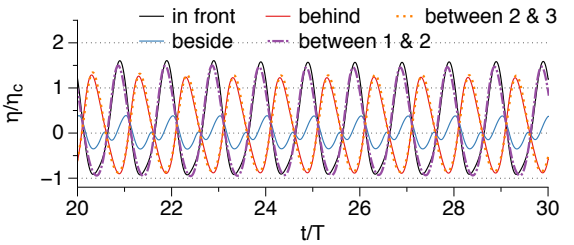

(d) cylinder 2, $H/L = 0.075$

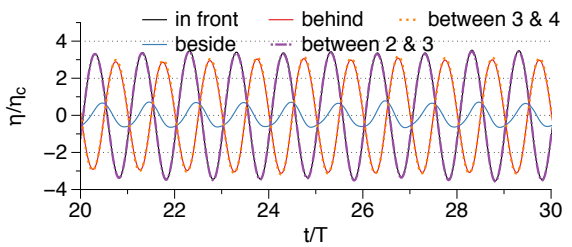

(e) cylinder 3, $H/L = 0.003$

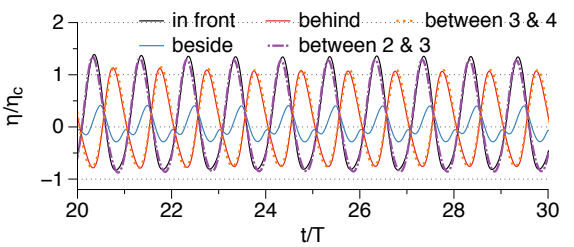

(f) cylinder 3, $H/L = 0.075$

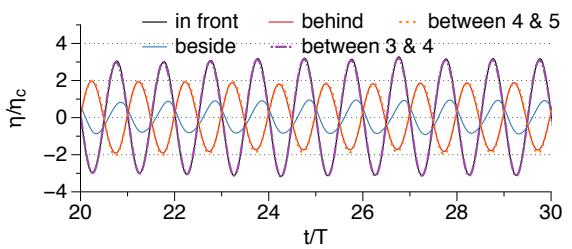

(g) cylinder 4, $H/L = 0.003$

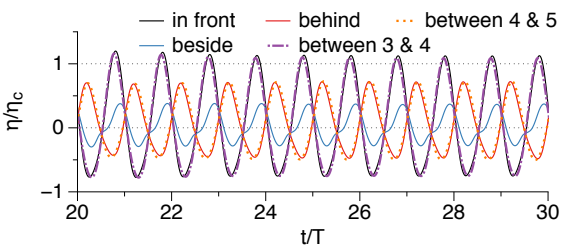

(h) cylinder 4, $H/L = 0.075$

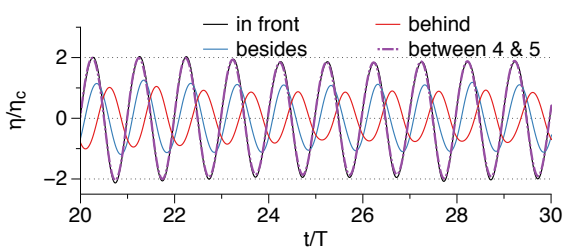

(i) cylinder 5, $H/L = 0.003$

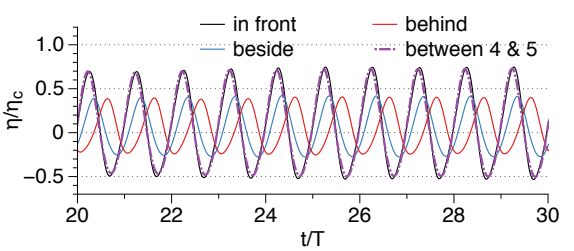

(j) cylinder 5, $H/L = 0.075$

Fig. 5: Variation of the free surface elevations in the vicinity of the cylinders for the five cylinder array at low and high steepness incident waves

are added downstream. It is also observed that the wave forces on the most downstream cylinder is lower than the force on a single cylinder in every case. The free surface elevations in the vicinity of the cylinders presented in Fig. (4) are studied to obtain more insight into the wave diffraction process in these cases. The free surface elevation contours in the vicinity of the cylinders in Fig (4) show that the free surface elevations constantly reduce along the length of the cylinder array. In addition, the formation of a large cylindrical wave is seen in front of the first cylinder in the array in every case, with a deep trough in the region behind it. This signifies that the largest pressure differences around the cylinders in the array occurs around the most upstream cylinder 1, resulting in the highest computed wave forces on cylinder 1. Large free surface elevations are seen between cylinders 2 and 3 in Figs. (4b), (4c) and (4d), but these elevations are lower than that seen in front of cylinder 1. This along with the shallower troughs behind the cylinders show that the pressure differences around these cylinders are lower and hence they experience lower forces than cylinder 1. The effect of diffraction significantly effects the wave field and the wavefront is deformed into two circular arcs intersecting behind the cylinders. The lowest pressure differences around the cylinders occurs in the vicinity of the most downstream cylinder in all the cases, signified by the lowest difference in the free surface elevation contours around it. As a result, the lowest forces in the array experienced by the most downstream cylinder in every case.

3.3. Comparison of low and high steepness wave interaction with a cylinder array

As seen from the previous sections, there are a few similarities and differences in the interaction of low and high steepness with cylinders. In both the cases, it is observed that the wave forces generally decrease along the length of the array. The exception is that in the low steepness cases, the cylinders towards the center of the array in arrangements with four and five cylinders experience the highest forces in the array. In the case of low steepness incident waves, the minimum force is experienced by the most downstream cylinder and the force is almost equal to the force on a single cylinder in all the cases simulated. In the case of the high steepness incident waves, although the most downstream cylinder experiences the minimum wave forces, the wave force is less than the force on a single cylinder in all the cases. This suggests that the diffraction effects are stronger for the higher steepness incident waves and the forces on the downstream cylinders are reduced significantly in comparison to the lower steepness incident waves. In both cases, however, the wave force on the most upstream cylinder in the array is increased with an increase in the number of cylinders added downstream of it.

The variation of the relative wave crest elevation over several wave periods in front, behind, near the wall along the center of the cylinder and in between the cylinders for the five cylinder array at low and high incident steepness is presented in Fig. (5). It is seen that in the case of the low steepness incident waves, the free surface elevations in front and behind every cylinder is more than two times the incident wave crest elevation, signifying the formation of standing waves in between the cylinders. In addition, the crest elevation in front and behind any cylinder is equal to the crest elevation at the midpoint between its closest upstream and downstream cylinder. The wave crest elevations near the wall are reduced due to the interaction of the diffracted waves.

In the case of the high steepness incident waves, the relative wave crest elevations are more than the incident crest elevation but less than $2\eta_c$ in all the cases. It is also noticed that wave crest elevations in front and behind the cylinder 5 are the lowest and also have the least difference between them in Fig. (5j), further validating the lowest forces in the array computed for it. A slight increase in the relative crest elevation is also seen as the wave propagates from the midpoint in the between two cylinder to in front of the next downstream cylinder. The crest elevations close to the wall are significantly deformed due to the strong diffraction effects and the formation of several radiating cylindrical waves seen in Fig. (4).

4. Conclusion

The open source CFD model, REEF3D was used to simulate the interaction of high and low steepness incident waves with a single cylinder and linear arrays of two, three, four and five cylinders. Several similarities and differences are observed between the interaction of low and high steepness waves with a linear array of cylinders. The diffraction effects are stronger for incident waves of higher steepness, resulting in significantly lower forces on the downstream cylinders in comparison to the lower steepness incident waves. The central cylinders in an array of more than three

cylinders experience the highest forces in the array for low steepness incident waves. Also, the formation of standing waves between the cylinders is observed in the case of low steepness incident waves. Further studies can be carried out to study the wave interaction with cylinder arrays with cylinders of different diameters and distance of separation.

Acknowledgements

This study has been carried out under the OWCBW project (No. 217622/E20) and the authors are grateful to the grants provided by the Research Council of Norway. This research was supported in part with computational resources at the Norwegian University of Science and Technology (NTNU) provided by The Norwegian Metacenter for Computational Science (NOTUR).

References

[1] M. Callan, C. M. Linton, D. Evans, Trapped modes in two-dimensional waveguides, Journal of Fluid Mechanics 229 (1991) 51–64.
[2] B. Spring, P. L. Monkmeyer, Interaction of plane waves with vertical cylinders, in: Proc., International Conference on Coastal Engineering, ASCE, Copenhagen, 1974, pp. 1828–1847.
[3] P. McIver, D. V. Evans, Approximation of wave forces on cylinder arrays, Applied Ocean Research 6 (1984) 101–107.
[4] C. M. Linton, D. V. Evans, The interaction of waves with arrays of vertical circular cylinders, Journal of Fluid Mechanics 215 (1990) 549–569.
[5] D. V. Evans, R. Porter, Near-trapping of waves by circular arrays of vertical cylinders, Applied Ocean Research 19 (1997) 83–99.
[6] D. A. G. Walker, R. E. Taylor, Wave diffraction from linear arrays of cylinders, Ocean Engineering 32 (2005) 2053–2078.
[7] B. J. S. Barnard, W. G. Pritchard, D. G. Provis, Experiments on wave trapping by a submerged cylindrical island, Geophysical and Astrophysical Fluid Dynamics 24 (1983) 23–48.
[8] H. Kagemoto, M. Murai, M. Saito, B. Molin, S. Malenica, Experimental and theoretical analysis of the wave decay along a long array of vertical cylinders, Journal of Fluid Mechanics 456 (2002) 113–135.
[9] G. Duclos, A. H. Clément, Wave propagation through arrays of unevenly spaced vertical piles, Ocean Engineering 31 (2004) 1655–1668.
[10] G. C. J. Morgan, J. Zang, D. Greaves, A. Heath, C. D. Whtilow, J. R. Young, Using the rasinterfoam CFD model for wave transformation and coastal modeling, in: Proc., Coastal Engineering Conference, Shanghai, China, 2010, pp. 1–9.
[11] N. G. Jacobsen, D. R. Fuhrman, J. Fredsøe, A wave generation toolbox for the open-source CFD library: OpenFOAM, International Journal for Numerical Methods in Fluids 70 (2011) 1073–1088.
[12] P. Higuera, L. J. Lara, I. J. Losada, Simulating coastal engineering processes with OpenFOAM, Coastal Engineering 71 (2013) 119–134.
[13] M. Alagan Chella, H. Bihs, D. Myrhaug, M. Muskulus, Breaking characteristics and geometric properties of spilling breakers over slopes, Coastal Engineering 95 (2015) 4–19.
[14] A. Kamath, M. Alagan Chella, H. Bihs, Ø. A. Arntsen, Cfd simulations of wave propagation and shoaling over a submerged bar, Aquatic Procedia 4 (2015) 308–316.
[15] A. Chorin, Numerical solution of the Navier-Stokes equations, Mathematics of Computation 22 (1968) 745–762.
[16] H. van der Vorst, BiCGStab: A fast and smoothly converging variant of Bi-CG for the solution of nonsymmetric linear systems, SIAM Journal on Scientific and Statistical Computing 13 (1992) 631–644.
[17] D. C. Wilcox, Turbulence modeling for CFD, DCW Industries Inc., La Canada, California., 1994.
[18] P. A. Durbin, Limiters and wall treatments in applied turbulence modeling, Fluid Dynamics Research 41 (2009) 1–18.
[19] D. Naot, W. Rodi, Calculation of secondary currents in channel flow, Journal of the Hydraulic Division, ASCE 108 (1982) 948–968.
[20] S. Osher, J. A. Sethian, Fronts propagating with curvature- dependent speed: algorithms based on Hamilton-Jacobi formulations, Journal of Computational Physics 79 (1988) 12–49.
[21] D. Peng, B. Merriman, S. Osher, H. Zhao, M. Kang, A PDE-based fast local level set method, Journal of Computational Physics 155 (1999) 410–438.
[22] G. S. Jiang, C. W. Shu, Efficient implementation of weighted ENO schemes, Journal of Computational Physics 126 (1996) 202–228.
[23] G. S. Jiang, D. Peng, Weighted ENO schemes for Hamilton-Jacobi equations, SIAM Journal on Scientific Computing 21 (2000) 2126–2143.
[24] H. Choi, P. Moin, Effects of the computational time step on numerical solutions of turbulent flow, Journal of Computational Physics 113 (1994) 1–4.
[25] P. A. Berthelsen, O. M. Faltinsen, A local directional ghost cell approach for incompressible viscous flow problems with irregular boundaries, Journal of Computational Physics 227 (2008) 4354–4397.
[26] A. Kamath, H. Bihs, Ø. A. Arntsen, Numerical modeling of power take-off damping in an oscillating water column device, International Journal of Marine Energy 10 (2015) 1–16.
[27] A. Kamath, M. Alagan Chella, H. Bihs, Ø. A. Arntsen, Evaluating wave forces on groups of three and nine cylinders using a 3D numerical wave tank, Engineering Applications of Computational Fluid Mechanics DOI:10.1080/19942060.2015.1031318 (2015).